Cation Coordination Polyhedra Lead to Multiple Lengthscale Organization in Aqueous Electrolytes

Yihui Wei,[*,†] Emily T. Nienhuis,[*,‡] Sebastian T. Mergelsberg,[‡] Trent R. Graham,[†] Qing Guo,[†] Gregory K. Schenter,[‡] Carolyn I. Pearce,[‡,¶] and Aurora E. Clark[*,†,‡]

†*Department of Chemistry, University of Utah, Salt Lake City, UT, USA*

‡*Pacific Northwest National Laboratory, Richland, WA, USA*

¶*Department of Crop and Soil Sciences, Washington State University, Pullman, WA, USA*

E-mail: yihui.wei@utah.edu; emily.nienhuis@pnnl.gov; aurora.clark@utah.edu

Abstract

Although long recognized, understanding multiple lengthscale correlations in the X-ray and neutron pair distribution functions of aqueous electrolytes remains a persistent challenge. This work leverages polyoxoanions to support cation-centric coordination polyhedra in $NaNO_{3(aq)}$ and $NaNO_{2(aq)}$ with characteristic pair-wise correlations interpreted through classical molecular dynamics simulations and graph-theoretical analyses. We demonstrate that the water oxygen Ow $\cdots$ Ow correlations associated with Na^+-coordination polyhedra (and their oligomers) have two characteristics lengthscales. That between 3.5 - 5.5 Å is associated with Ow coordinated to the same Na^+, while the second between 5.5 - 7.5 Å is associated with Ow coordinating different Na^+ connected by bridging anions, corner-, edge-, or face-sharing. The ubiquitous contraction of the PDF between 5.5 - 7.5 Å observed in many electrolytes derives from the loss of the

many-body bulk Ow $\cdots$ Ow and growth of all combinations of Ow and On correlations that emerge due to the ion network of Na-coordination polyhedra.

Many properties of aqueous electrolytes are directly attributed to, or strongly correlated with, structural organization of the solution. Conductivity,[1,2] diffusion[3] and transport properties[4] depend upon local speciation and organization, while complex and unresolved relationships exist between the solution structure and varying aspects of phase behavior (e.g., solubility,[5–7] nucleation mechanisms,[8] and particle aggregation[9]). The total pair distribution function (PDFs, also referred to as G(r)) obtained from either X-ray or neutron total scattering, is a primary technique used to evaluate solution structure, where multiple length scale correlations are observed. At a local-scale, significant study has been dedicated to elucidating ion-solvation structures (solvation numbers and geometries), ion speciation (contact ion pairs (CIPs) and solvent separated ion pairs (SSIPs)), and specific ion effects upon the bulk water structure.[10–15] While most emphasis has historically been towards relatively dilute concentration regimes, highly concentrated (so-called $water-in-salt$ solutions) have recently grown in importance due to emerging aqueous battery technologies[1,2,16,17] and challenges in the processing of industrial wastes (including nuclear waste management).[9,18,19] As the solubility limit is approached, there is insufficient H_2O to form complete solvation shells about ions causing increases to CIPs and SSIPs.[11,18] Concomitantly, pair correlations in the PDF emerge at two characteristic distance regimes that represent changes to the 2^{nd} nearest neighbor interactions at 3.5 - 5.5 Å (the **mid-range**) and the 3^{rd} - 4^{th} neighbor at approximately 5.5 - 7.5 Å (the **long-range**).

Elucidating the origin of mid-range organization is a significant challenge as it may result from overlapping atom-pair correlations.[20–24] This problem is amplified in the long-range and as the solution complexity and electrolyte concentration are increased. Assuming a spherical shell model of solvation, the change in volume increases as $\frac{4}{3}\pi r^3$ and in moving from the mid- to the long-range regime the number of accommodating H_2O nearly doubles with an $N(N-1)/2$ increase in pairs. Mid-range O-O pair correlations for water (Ow$\cdots$Ow)

occur between 3.5 - 5.5 Å (centered at 4.5 Å)[25,26] but overlap with ion$\cdots$O distances for many halides (2.8 - 3.6 Å) and polyoxoanions (3.7 Å for NO_2^- or NO_3^- and 4.3 Å for SO_4^-). Depending on the electrolyte identity and concentration, the mid-range peak centered at 4.5 Å may thus have an overall decrease in intensity with increasing electrolyte concentration (commensurate with a loss of Ow$\cdots$Ow pairs) or it may also change its location or shape as contributions from Ow$\cdots$ion correlations increase their prevalence.

The contributions at long-range reflect a distribution of many-body configurations often described by geometric metrics (angular distributions) or local water density. Interestingly, the trends in G(r) as a function of electrolyte concentration are similar to those observed for water under increasing pressure, leading to similar structural interpretations.[27,28] Upon compression from 1 to 3000 bar, the 2^{nd} shell Ow$\cdots$Ow correlation contracts from 4.5 to to $\sim$ 4.3 Å with a significant decrease in intensity.[29] Meanwhile the 3^{rd} shell long-range correlation contracts and the interstitial space in between the mid- and long-range increases in intensity. Structural models of water at high-P propose a collapse of the 2^{nd} solvation shell about individual H_2O that expels them and causes higher occupancy in the interstitial space with the 3^{rd} shell concomitant with an increase in the bulk water density.[28–31] This may lead to increased orientation disorder.[27,32] The PDFs of $NaCl_{(aq)}$ exhibit similar changes as concentration is increased. The mid-range Ow$\cdots$Ow correlation exhibits a slight distance *increase* alongside a similar decrease in the peak intensity and the contraction of the long-range correlation is more pronounced than in P-dependent pure water. Originally thought to come from similar structural origins, recent work has instead indicated an intrinsically different molecular origin in the concentration dependent electrolytes; changes to the mid- and long-range G(r) primilarly derive from the H_2O that reside in the 1^{st} solvation shell of Na^+ *and* Cl^- rather than shifting waters of solvation between 2^{nd} - 3^{rd} shells.[29]

Amidst emerging structural interpretations of mid-range correlations, little has been proposed regarding the structural origins of long-range correlation. Contraction of the long-range feature in the PDF is more ubiquitous and less ion-dependent than changes to the

mid-range.[10,18,29,33,34] The breadth of configurational phase space has led to interpretation based upon contributing atom-pair types rather than molecular configurations or organizational metrics.[10] Yet approaches that relate atom-pair correlations to an ensemble of structurally organized "states" would be an important stepping stone to achieve a comprehensive understanding of the relationships between solution structure and the molecular underpinnings of phase phenomena and solution properties. Intriguingly, prior analysis of the PDF and radial distribution functions (RDFs) of concentrated $NaOH_{(aq)}$[15,35] has indicated the presence of extended (but highly fluxional) ion-networks of connectivity, where the solvation or coordination to both Na^+ and OH^- strongly influence the PDF. We hypothesize in this work that the ion-networks may be stabilized by polyoxo anions like NO_2^- and NO_3^- whose binding modes to Na^+ and other metals[14,36] lead to readily identifiable geometric arrangements across lengthscales. Additionally, the solvation environments about polyoxoanions are less organized than to Na^+ and as such the analysis of ion-networks may be viewed through a cation-centric framework that focuses solely upon the polyhedral coordination environment to Na^+.

Toward this end, we examine the structure of solutions of $NaNO_2$ and $NaNO_3$ at 1 m, 2.5 m, 4 m, 6 m, 8 m, 10 m, and saturation. X-ray PDFs were obtained through X-ray total scattering measurements at the Advanced Photon Source, beamline 11-ID-B. Calibration and data reduction were performed using GSAS-II.[37] Data was background subtracted to remove contributions from air scattering and from the capillary, Fourier transformed, and normalized using PDFGetX2.[38] These experimental studies are complemented by ab initio and classical molecular dynamics (CMD) simulations and detailed graph-theoretical analysis of the intermolecular interaction networks. The CMD simulations employed benchmarked force fields for the entire concentration range and were used to produce simulated X-ray G(r) using the DISCUS software program[39] and RDFs that identify key correlations at specific distances. RDFs for specific atom types over the entire simulationensemble are labelled g(r) and calculated using Eqn. S3, while RDFs for sub-ensembles (groups of atom types) are

referred to as g'(r) and calculated using Eqn. S4. Additional details regarding experimental and computational methods and analyses are available in the Supporting Information.

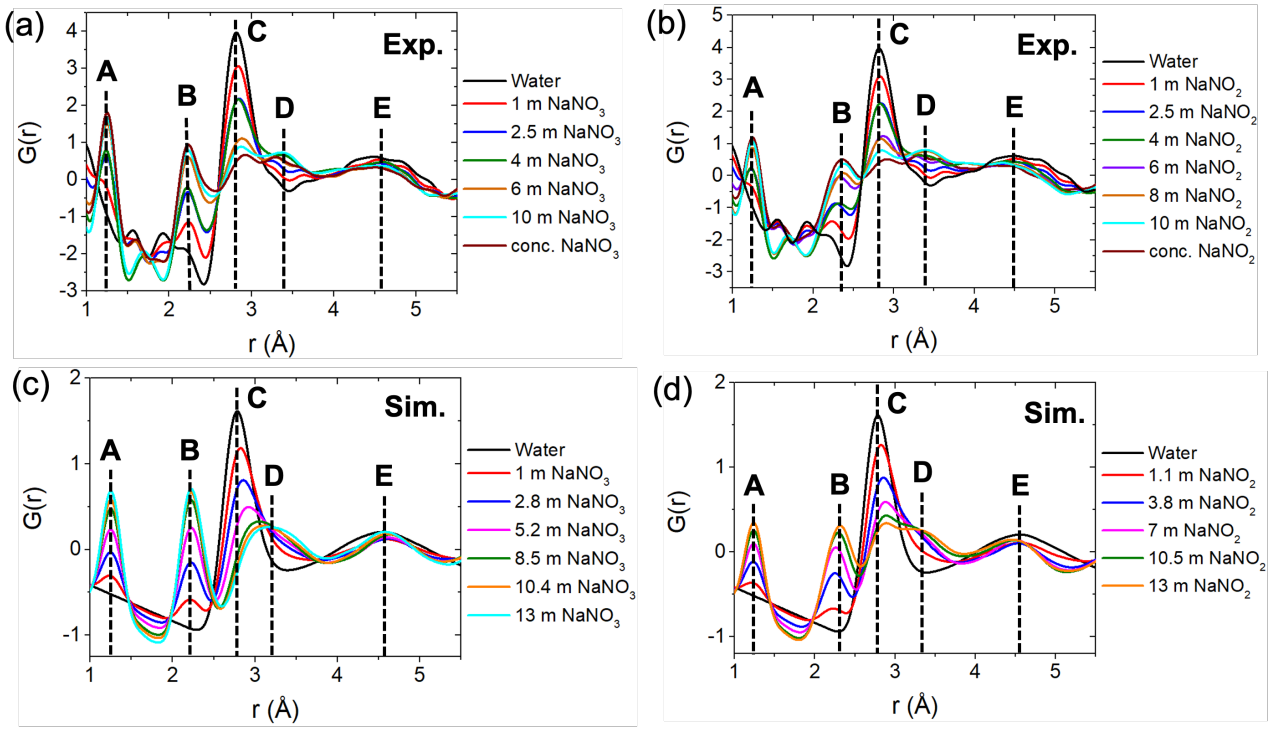

Figure 1: (a) Experimental X-ray PDF for concentration dependent $NaNO_{3(aq)}$ up to 5.5 Å. (b) Experimental X-ray PDF for concentration dependent $NaNO_{2(aq)}$ up to 5.5 Å. (c) Simulated X-ray PDF for $NaNO_{3(aq)}$ solutions obtained using DISCUS[39] in the mid-range. (d) Simulated X-ray PDF for $NaNO_{2(aq)}$ solutions obtained using DISCUS in the mid-range.

Table 1: Pairwise contributions to features **B** - **E** in $NaNO_{3(aq)}$ and $NaNO_{(2(aq)}$ simulated PDFs at select distances as identified from the CMD RDFs presented in Figures S5 - S7.

Feature	$NaNO_{3(aq)}$			$NaNO_{2(aq)}$		
B	$O_N \cdots O_N$	$Na \cdots Ow$	$Na \cdots O_N$	$O_N \cdots O_N$	$Na \cdots Ow$	$Na \cdots O_N$
	2.18 Å	2.25 Å	2.48 Å	2.08 Å	2.26 Å	2.46 Å
C - D	$Ow \cdots Ow$		$Ow \cdots O_N$	$Ow \cdots Ow$		$Ow \cdots O_N$
	2.78, 3.14 Å		2.92 Å	2.78, 3.1 Å		2.81 Å
E	$Ow \cdots Ow$		$Ow \cdots O_N$	$Ow \cdots Ow$		$Ow \cdots O_N$
	4.5 Å		4.68 Å	4.56 Å		4.58 Å

Within the experimental and simulated G(r) of $NaNO_{3(aq)}$ and $NaNO_{2(aq)}$, well-defined features are observed into the mid-range that complement significant changes to the local-coordination or solvation environments and speciation observed in the CMD simulations.

In Figure 1, three nearest-neighbor features are observed that are consistent with prior reports.[40] The experimental feature **A** at $\sim$ 1.25 Å is associated with the intramolecular oxyanion N-O bond. Feature **B** occurs at $\sim$ 2.23 Å in $NaNO_3$ and 2.23 - 2.39 Å in $NaNO_2$ dependant on concentration. At 1 m $NaNO_2$, **B** is centered at 2.48 Å and 1 m $NaNO_3$ at 2.40 Å (2.23 Å and and 2.21 Å in the simulated PDF). This feature broadens and shifts to longer distances with increased [$NaNO_x$]; at saturated conditions the experimental **B** has broadened by 0.13 Å and shifted by 0.16 Å for $NaNO_{2(aq)}$, and in $NaNO_{3(aq)}$ it has broadened by 0.07 Å (with no change to the peak position). As observed Table 1, Na$\cdots$O and $O_N\cdots O_N$ correlations align with PDF feature **B** (shown in Figure S5).[41] In the case of $NaNO_{3(aq)}$, there is significant overlap in the $O_N\cdots O_N$ and Na$\cdots$Ow correlations (centered at 2.18 Å and 2.25 Å, respectively) both of which gain intensity as [$NaNO_3$] is increased. In contrast, the overlap in the $O_N\cdots O_N$ (centered at 2.08 Å) and Na$\cdots$Ow (centered at 2.26 Å) is much smaller in $NaNO_{2(aq)}$ and more significant overlap is observed between Na$\cdots$Ow and Na$\cdots O_N$ (centered at 2.46 Å). These data are consistent with the changes to the local coordination environment about Na^+, including increased ion pairing (direct anion coordination) that is observed in the CMD simulation as a function of electrolyte concentration. This includes the number of nitrates bound to Na^+ as well- trends in denticity of the anion to Na^+. Figure 2a presents the most observed coordination environments about Na^+ as a function of concentration, while Table S5 presents exact % observation and Table S6 presents the distributions of anion binding modes. Ab-initio potential of mean force simulations of the change from bidentate to monodentate NO_3^- and NO_2^- bound to a single Na^+ indicate two well-defined minima for each coordination state for NO_2^-, while no barrier is observed between the two states for NO_3^- (Figure S8). At low electrolyte concentration this manifests itself in the benchmarked CMD as similar observations of bi- and monodentate coordination in [$NaNO_2$] while monodentate coordination is observed at low concentrations of [$NaNO_3$]. With increasing electrolyte concentration bidentate coordination increases for both systems and there is a substantial increase of mono- then di- and tri-nitrate species as

ion-pairing is enhanced. These two phenomena underpin the increased contributions of the $O_N \cdots O_N$ and $Na \cdots O_N$ within this region for both systems.

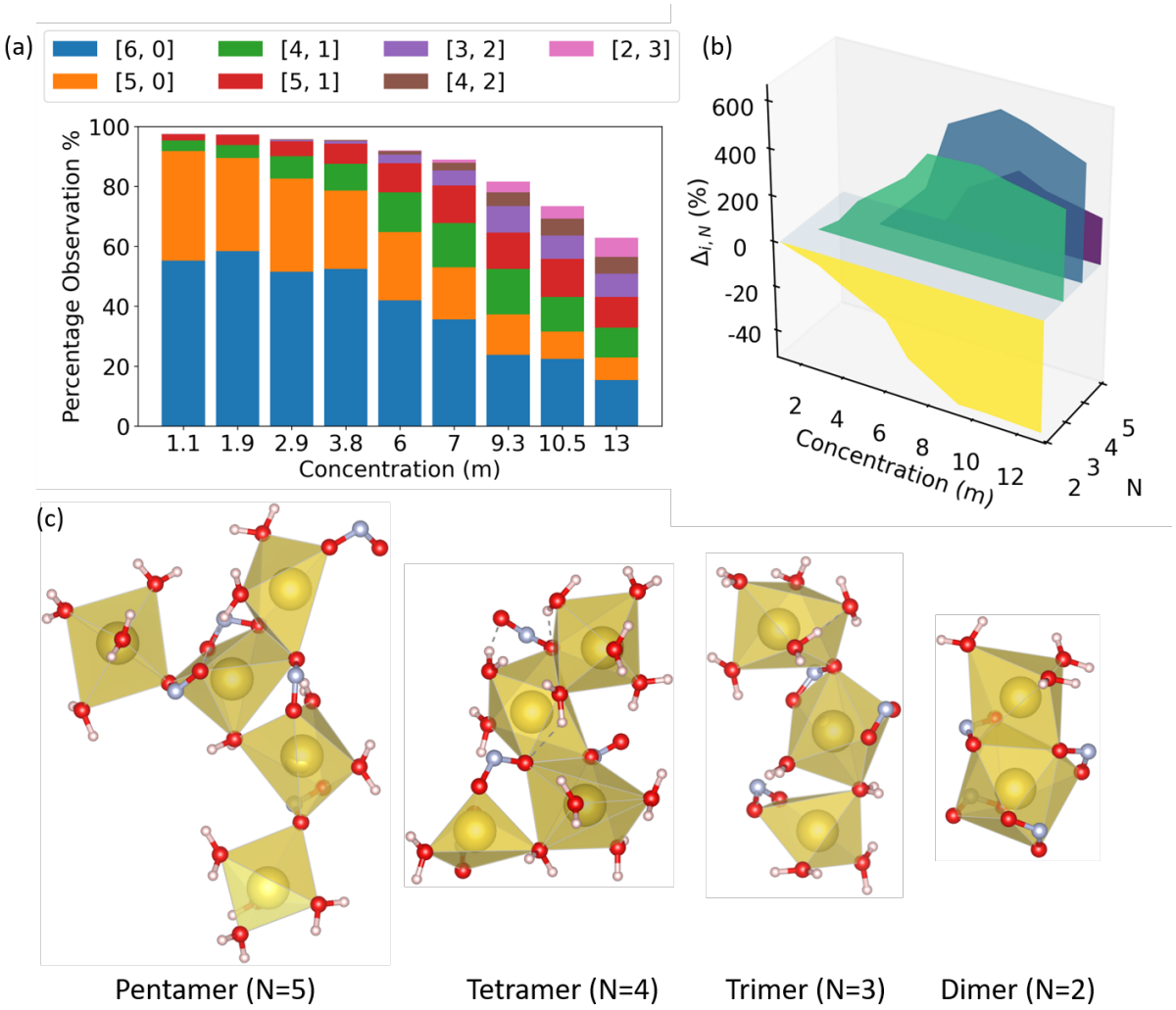

Figure 2: (a) Percent observation of coordination environment of Na^+ as a function of [$NaNO_2$]. Labels [a, b] indicates number of coordinated H_2O and NO_2^-. Number distribution provided in Table S7. Only the top six coordination environments are plotted here. (b) The % change $\Delta_{i,N}$ of Na^+ coordination polyhedron and their oligomers of size N as a function [$NaNO_2$]. $\Delta_{i,N} = (P_{i,N} - P_{c,N})/P_{c,N}$, where P is the probability of observation at at a concentration i relative to the lowest concentration c for which N-oligomer size is observed. The decrease in observation of N = 3 - 5 at high [$NaNO_2$] is attributed to highly fluxional large N that occur at low frequency and are not reported. Number distribution provided in Table S8. (c) Examples of oligomers in $NaNO_2$ solutions. This information for $NaNO_3$ solutions are shown in Figure S10.

The third feature in the experimental G(r), labelled **C**, is centered at 2.82 Å at 1 m

$NaNO_{3(aq)}$ and $NaNO_{2(aq)}$, and in the RDFs align with Ow $\cdots$ Ow and Ow$\cdots$ O_N correlations. Apriori it should be recognized that the number and strength of the hydrogen bonds (HBs) differs between the anions, which has a significant affect upon Ow$\cdots$ O_N distance dependent correlations.[42] In NO_3^-, the three O atoms are HB acceptors;[42] in the case of NO_2^-, the two O atoms and the central N-atom act has HB acceptor sites. NO_2^- additionally exhibits asymmetry towards its hydrogen bonding, with a stronger interaction between nitrogen and water than the oxygen sites.[43] The differences in interaction between the NO_3^- and NO_2^- with solvating H_2O are reflected in the average of Ow$\cdots$ O_N g(r) distances of 2.92 and 2.81 Å respectively (Figure S6), concomitant to higher viscosities in aqueous NO_2^- relative to NO_3^-.[44]

Given these data, one might anticipate concentration dependent shifts to **C**. Indeed, **C** decreases in intensity and shifts by 0.1 Å to longer distance with increasing electrolyte while a neighboring feature **D** at c.a. 3.5 Å increases in intensity. As shown in Figure S6, in both $NaNO_{3(aq)}$ and $NaNO_{2(aq)}$ the Ow $\cdots$ Ow RDFs within 2.78 - 2.82 Å decreases in intensity (decreased concentration of these pairs) as the electrolyte concentration is increased, yet concomitantly a new Ow $\cdots$ Ow correlation centered at 3.12 Å (in between **C** and **D**) emerges. At saturation the two distinct Ow $\cdots$ Ow correlations have approximately the same intensity (yet they are both smaller than the single contribution observed at $\sim$ 1 m conditions). Thus, for both solutions the Ow $\cdots$ Ow correlation g(r) decrease in intensity, broaden and shift to longer distance with increasing electrolyte concentration. A differentiating factor between the two electrolytes is the Ow $\cdots$ O_N correlation, which has two distinct distances in the RDF depending on the anion; in $NaNO_{3(aq)}$ the distance is 2.92 Å while it is shorter at 2.81 Å in $NaNO_{2(aq)}$. Feature **D**, which appears as a shoulder to **C** in the G(r), is attributed primarily to the new Ow $\cdots$ Ow at 3.1 Åin g(r), whose origin is not apparent (*vide infra*). In contrast, for $NaNO_{3(aq)}$ there is a slightly larger distance separation between the Ow $\cdots$ Ow g(r) correlation at 2.8 Å and the Ow $\cdots$ O_N at 2.92 Å. The concentration dependent changes to **C - D** are slightly more exaggerated in the simulated PDF relative to experiment, however the same trend is observed in both.

The final mid-range feature, **E**, in G(r) is broad and at 1 m begins at $\sim$ 3.48 Å and extends to 5.73 Å with the peak centered at $\sim$ 4.53 Å in Figure 1. As shown in Figure S7, the Ow $\cdots$ Ow g(r) (centered at 4.5 - 4.56 Å) and Ow $\cdots$ O_N (centered at 4.68 Å and 4.58 Å for $NaNO_{3(aq)}$ and $NaNO_{2(aq)}$, respectively) align with **E**. With increasing [$NaNO_x$], the emergence of **D** obscures the start of **E** and there is considerable overlap of the two features at 4 Å. Experimentally, the range of **E** contracts; in concentrated $NaNO_{3(aq)}$ (Figure 1a), **E** ends at c.a. 5.32 Å which represents a contraction of nearly 0.4 Å. Similar behavior is observed in concentrated $NaNO_{2(aq)}$ (Figure 1b) where **E** ends at approximately 5.19 Å. Thus the range of **E** contracts significantly in both electrolytes, but with a more pronounced change in $NaNO_{2(aq)}$. Although there is no distinct shift in the experimental position of the peak maximum for $NaNO_{3(aq)}$, in $NaNO_{2(aq)}$ the peak shifts from $\sim$ 4.53 Å in the 1 m solution to 4.40 Å at saturation. In the simulated g(r) the range of Ow $\cdots$ Ow contributions similarly become more narrow as concentration is increased and at the same time the Ow $\cdots$ O_N contributions increase which is shorter in $NaNO_{2(aq)}$ relative to $NaNO_{3(aq)}$. Like peak **D**, an interpretation of **E** based upon the local anion or water coordination to Na^+ is not obvious.

Although the trends to the experimental PDF are similar to those observed in other systems like $NaCl_{(aq)}$, the interplay of features **C** - **D** and shift of **E** indicate that there may exist local *molecular* organizational motifs that are building blocks for extended solution structure. The trends in anion coordination to Na^+ are one key indicator. As shown in Figure 2a and Table S6 there is significant growth of the number of anions bound to Na^+. Those anions not participating in such ion-paired species at high concentrations are all part of SSIPs. The large concentration of di- and trinitrate bound structures is a strong indicator of longer lengthscale ion interactions. With this perspective, we now focus upon the long-range correlations observed between 5.5 - 7.5 Å as shown in Figure 3.

At 1 m, feature **G** occurs at $\sim$ 6.84 Å. Yet as [$NaNO_x$] increases **G** decreases in intensity and there is a distinct shift to yield feature **F**, centered at 6.15 and 6.23 Å at saturated

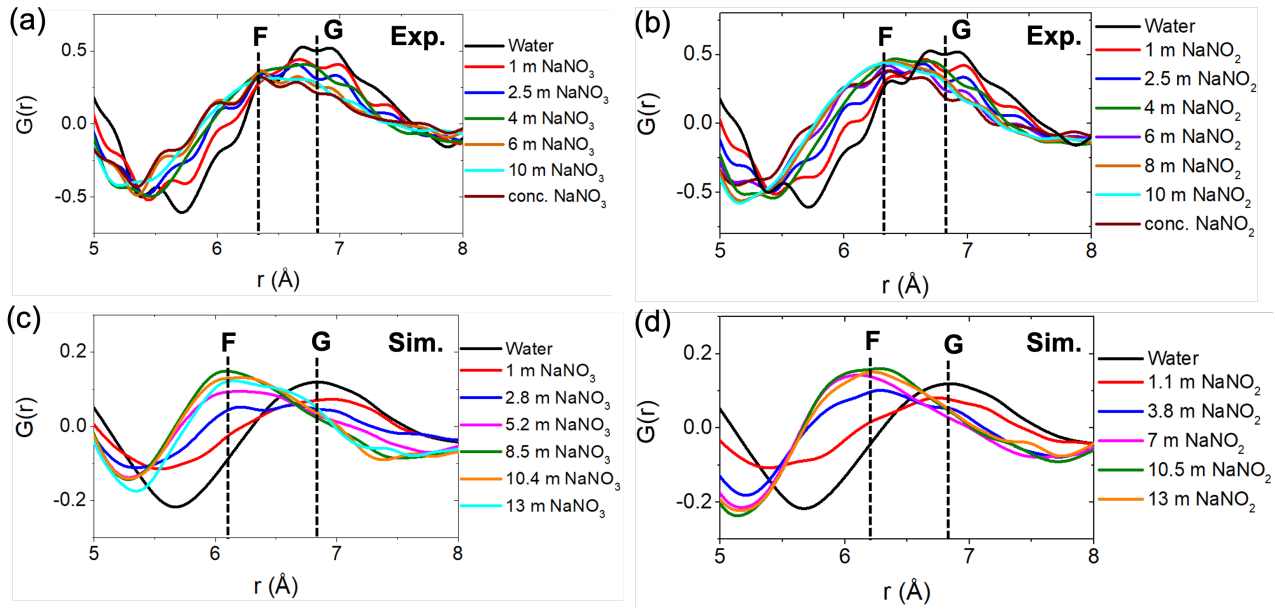

Figure 3: (a) Experimental X-ray PDF for $NaNO_3$ solutions with emphasis on long-range features. (b) Experimental X-ray PDF for $NaNO_2$ solutions with emphasis on long-range features. (c) Simulated X-ray PDF for $NaNO_3$ solutions from DISCUS.[39] (d) Simulated X-ray PDF for $NaNO_2$ solutions from DISCUS.

$NaNO_{3(aq)}$ and $NaNO_{2(aq)}$, respectively. The simulated PDFs reproduce this trend, with Ow $\cdots$ Ow and Ow $\cdots$ O_N correlations having significant concentration of in this distance region in the RDF. Prior study of $NaNO_{3(aq)}$ has interpreted this trend qualitatively through the disruption and replacement of Ow $\cdots$ Ow by Ow $\cdots$ O_N.[40] More quantitatively, at least two different structural models could be put forward. First, small variations in HB distances or angles (not resolved by the PDF) may propagate to longer lengthscales and lead to the observed contraction. As observed in Figure S11 and Table S9, variations in HB distance of 0.1 Å and 10 ° easily lead to shift in Ow $\cdots$ Ow distances of 0.3 Å in the mid-range. Extending such logic to the 4 - 5 hydrogen bond pathways needed to get to the long-range distance region is entirely consistent with the alteration of **G** to **F**. Thus, in *structural model 1* the long-range contraction is an emergent behavior that derives from subtle variations in intermolecular interactions of pairs of H_2O. In *structural model 2*, the bulk water network is systematically replaced by coordination polyhedra about Na^+, where new Ow $\cdots$ Ow correlations emerge when multiple water solvate the same Na^+, are constrained in between

Na^+ as part of SSIPs, and form new Ow $\cdots$ O_N correlations when an H_2O and NO_3^- or NO_2^- coordinate to the same Na^+. Connected coordination polyhedra of Na^+ may also lead to new Ow $\cdots$ Ow and Ow $\cdots$ O_N correlations depending on the nature of the connectivity. The second structural model thus provides a "molecular" building block model of extended ion-network connectivity from a cation-centric perspective. To discern between the two structural models, graphs of intermolecular interactions were employed to identify: 1) the ensemble distribution of local coordination environments to Na^+ including the composition, polyhedral geometry, and any oligomerization; 2) different H_2O and their hydrogen bonding patterns outside of any interactions to the electrolyte ions.

Referring to the first analysis, as illustrated in Figure 2a, the composition of the coordination environment about Na^+ becomes increasingly complex with increasing electrolyte concentration. At saturation only $\sim$ 60 % of the coordination to Na^+ is described by "traditional" ratios of coordinated H_2O and anion where the anion is bound to a single Na^+ in a mono- or bidentate fashion. Instead, there is a huge increase of anion coordination to multiple Na^+ within an oligomeric framework, characterized using the terminology of Reference 45. As shown in Table S5 bidentate κ^2 anion coordination to 2 Na^+ is observed in $\sim$ 5% concentrations even at 1 m electrolyte concentration. Yet significant growth of tridentate μ_2-κ^2:κ^1 anion coordination begins to be observed at 6 m [$NaNO_{3(aq)}$] and 10.4 m [$NaNO_{2(aq)}$]. As saturation is reached in both cases, a large breadth of tetra up to heptadentate anion coordination modes are observed. Necessarily anion coordination to multiple Na^+ ions means oligomerization of the coordination polyhedra illustrated in Figure 2b. The anion may bridge coordination polyhedra or participate in corner-sharing, however coordinated H_2O may additionally participate in edge- and face-sharing connectivity patterns (illustrated in Figure S12). Representative oligomeric struftures are shown in Figure 2c. Anion bridging and corner-sharing connectivity are the most frequently observed, followed by edge- and face-sharing (Table S10). Although there is always a predominance of dimers in the solution, there is growth of up to hexamers at appreciable concentrations near saturation. Note

too that near saturation these more stable oligomers appear to exist in a highly fluxional near-percolated network of ion-interactions.

With the speciation of all Na^+ coordination environments and oligomers of coordination polyhedra identified, we now turn to the contributions of the O$\cdots$O correlations that derive from the polyhedral building blocks of ion connectivity, relative to the H_2O that do not interact with any ions that represent a "bulk water" state. This is done by analyzing the positions of partial RDFs g'(r) of these groups of atom types. As shown in Figure 4, within the mid-range, the Ow $\cdots$ Ow correlation of the bulk water state is centered at 2.78 Å and does not change position as a function of electrolyte concentration. The Ow that reside purely within the coordination polyhedra of Na^+ and network of connected polyhedra have a peak centered at 3.16 Å for $NaNO_{2(aq)}$ and at 3.15 Å for $NaNO_{3(aq)}$. This correlation of Ow does not change position with increasing electrolyte concentration. Finally, the waters that lie at the interface of the coordination polyhedron network and the bulk water network were examined to assess any variations in Ow$\cdots$Ow correlation. In fact, these waters have structural correlations remarkably similar to the bulk and as such are ignored in future analyses.

Turning to the interpretation of the long-range correlations in the experimental G(r), Figure 4(c) and (d) present the O$\cdots$O RDFs for the two structural models. The Ow $\cdots$ Ow correlations of the bulk water state, centered at 6.85 and 6.75 Å for $NaNO_3$ and $NaNO_2$ respectively, agree with feature **G** in Figure 1, while the general O$\cdots$ O (containing the mixture of all Ow and O_N correlations) associated with the network of connected Na-coordination polyhedra has a peak maximum at 6.25 and 6.15 Å for $NaNO_3$ and $NaNO_2$ respectively aligning with feature **F** in Figure 1. To learn more about the nature of the change in the Ow $\cdots$ Ow correlations, we plot in Figure S14 the shortest path of all interactions (hydrogen bonding, ion$\cdots$Ow, etc) between all Ow in the entire systems. While the most probably interactions pathways of water are in the range of 2 - 10, a steady decrease of the longer paths is observed with increasing electrolyte concentration. Interaction pathways of length 4

are preferentially increased in the network of all Ow interactions concomitant to the growth of the connectivity of Na^+ coordination polyhedra.

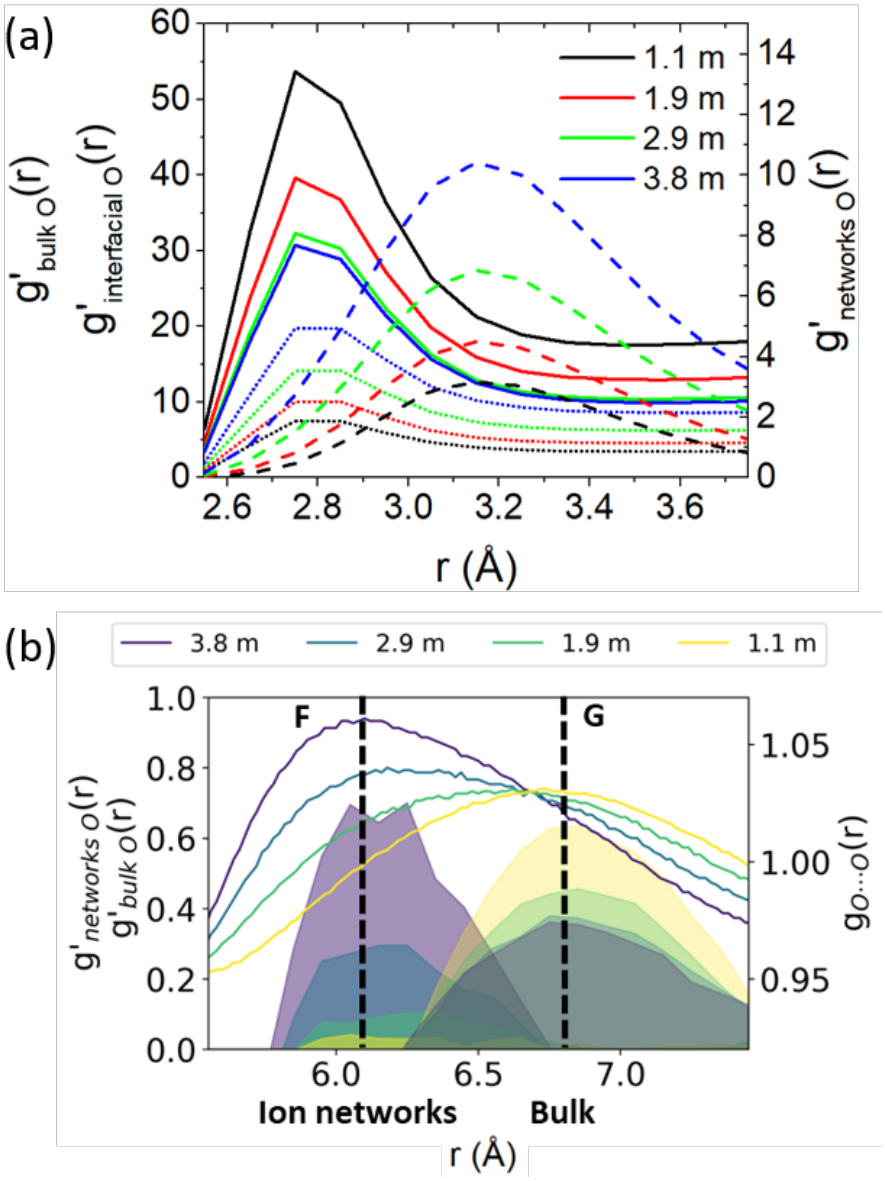

Figure 4: (a) Partial RDFs of different oxygen states in $NaNO_2$ solutions at short-range. Solid lines: bulk O $\cdots$ O; dash lines: networks O $\cdots$ O; dot lines: interfacial O $\cdots$ O. (b) O$\cdots$O RDFs (solid lines) and partial RDFs of different oxygen states (shaded lines, calculated using Eqn. S4) in $NaNO_2$ solutions at long-range. g'(r) are aligned by moving the averaged g'(r) from 5.5-7.5 Å to 0. Partial RDFs of $NaNO_3$ solutions are shown in Figure S13.

In combination, these data indicate that connected cation-centric coordination polyhedra (facilitated by polyoxoanions) form a basis for interpretation of atom correlations across lengthscale in experimental PDFs. The experimental changes to G(r) of concentration dependent $NaNO_{3(aq)}$ and $NaNO_{2(aq)}$ indicate two significant conceptual advances to our understanding of multiple lengthscale solution organization. First, we demonstrate that the Ow $\cdots$ Ow correlations associated with ion solvation, and more explicitly oligomerization of the coordination polyhedra about a metal cation have two characteristics lengthscales. The first occurs in the mid-range distance and is associated with Ow within the coordination shell about the same cation, while the second occurs at long-range distance and is associated with Ow coordinating different cations connected by bridging anions, corner-, edge-, or face-sharing. The second conceptual advance is that the general contraction of the long-range feature, observed ubiquitously across many aqueous electrolytes, can be explained in the $NaNO_{3(aq)}$ and $NaNO_{2(aq)}$ systems as deriving from the loss of the many-body bulk water correlation and growth of ion-network O $\cdots$ O correlation comprised of all combinations of Ow and On correlations facilitated by paths of pair-wise interactions that have defined characteristics due to the ion network of coordination polyhedra.

Acknowledgement

This research was supported by IDREAM (Interfacial Dynamics in Radioactive Environments and Materials), an Energy Frontier Research Center funded by the U.S. Department of Energy (DOE), Office of Science, Basic Energy Sciences. PNNL is a multiprogram national laboratory operated for DOE by Battelle Memorial Institute under Contract No. DE-AC05-76RL0-1830. This research used resources of the Advanced Photon Source, a U.S. Department of Energy (DOE) Office of Science user facility operated for the DOE Office of Science by Argonne National Laboratory under Contract No. DE-AC02-06CH11357.

Supporting Information Available

The following files are available free of charge.

- PDFgetX2-processing-example.gr: X-ray total scattering experimental details and data processing
- Supplementary Information: Containing detailed information regarding experimental setup and computational methodology as well as additional information regarding the key distributions of species supporting the interpretation of the X-ray PDF.

References

(1) Kim, H.; Hong, J.; Park, K.-Y.; Kim, H.; Kim, S.-W.; Kang, K. Aqueous rechargeable Li and Na ion batteries. *Chemical reviews* **2014**, *114*, 11788–11827.

(2) Kuhnel, R.-S.; Reber, D.; Battaglia, C. A high-voltage aqueous electrolyte for sodium-ion batteries. *ACS Energy Letters* **2017**, *2*, 2005–2006.

(3) Reynolds, J. G.; Graham, T. R.; Pearce, C. I. Ion hydration controls self-diffusion in multicomponent aqueous electrolyte solutions of NaNO2-NaOH-H2O. *Journal of Molecular Liquids* **2022**, 119441.

(4) Yadav, S.; Chandra, A. Transport of hydrated nitrate and nitrite ions through graphene nanopores in aqueous medium. *Journal of Computational Chemistry* **2020**, *41*, 1850–1858.

(5) Hofmeister, F. On the understanding of the effects of salts. *Arch. Exp. Pathol. Pharmakol.(Leipzig)* **1888**, *24*, 247–260.

(6) Thosar, A. U.; Patel, A. J. Hydration determines anion accumulation. *Nature Chemistry* **2022**, *14*, 8–10.

(7) Pegram, L. M.; Record Jr, M. T. Thermodynamic origin of Hofmeister ion effects. *The journal of physical chemistry B* **2008**, *112*, 9428–9436.

(8) Fetisov, E. O.; Mundy, C. J.; Schenter, G. K.; Benmore, C. J.; Fulton, J. L.; Kathmann, S. M. Nanometer-scale correlations in aqueous salt solutions. *The Journal of Physical Chemistry Letters* **2020**, *11*, 2598–2604.

(9) Anovitz, L.; Huestis, P.; Rampal, N.; Stack, A.; LaVerne, J.; Zhang, X.; Schenter, G.; Chun, J.; Legg, B.; Liu, L., et al. Frustrated Coulombic and Cation Size Effects on Nanoscale Boehmite Aggregation: A Tumbler Small-and Ultra-Small-Angle Neutron Scattering Study. *The Journal of Physical Chemistry C* **2022**, *126*, 4391–4414.

(10) Bouazizi, S.; Nasr, S.; Jaîdane, N.; Bellissent-Funel, M.-C. Local order in aqueous NaCl solutions and pure water: X-ray scattering and molecular dynamics simulations study. *The Journal of Physical Chemistry B* **2006**, *110*, 23515–23523.

(11) Wang, H.-W.; Vlcek, L.; Neuefeind, J. C.; Page, K.; Irle, S.; Simonson, J. M.; Stack, A. G. Decoding oxyanion aqueous solvation structure: A potassium nitrate example at saturation. *The Journal of Physical Chemistry B* **2018**, *122*, 7584–7589.

(12) Mason, P. E.; Tavagnacco, L.; Saboungi, M.-L.; Hansen, T.; Fischer, H. E.; Neilson, G. W.; Ichiye, T.; Brady, J. W. Molecular Dynamics and Neutron Scattering Studies of Potassium Chloride in Aqueous Solution. *The Journal of Physical Chemistry B* **2019**, *123*, 10807–10813.

(13) Balos, V.; Imoto, S.; Netz, R. R.; Bonn, M.; Bonthuis, D. J.; Nagata, Y.; Hunger, J. Macroscopic conductivity of aqueous electrolyte solutions scales with ultrafast microscopic ion motions. *Nature communications* **2020**, *11*, 1–8.

(14) Xie, W. J.; Zhang, Z.; Gao, Y. Q. Ion pairing in alkali nitrate electrolyte solutions. *The Journal of Physical Chemistry B* **2016**, *120*, 2343–2351.

(15) Semrouni, D.; Wang, H.-W.; Clark, S. B.; Pearce, C. I.; Page, K.; Schenter, G.; Wesolowski, D. J.; Stack, A. G.; Clark, A. E. Resolving local configurational contributions to X-ray and neutron radial distribution functions within solutions of concentrated electrolytes–a case study of concentrated NaOH. *Physical Chemistry Chemical Physics* **2019**, *21*, 6828–6838.

(16) Zhang, H.; Liu, X.; Li, H.; Hasa, I.; Passerini, S. Challenges and strategies for high-energy aqueous electrolyte rechargeable batteries. *Angewandte Chemie International Edition* **2021**, *60*, 598–616.

(17) Chen, L.; Zhang, J.; Li, Q.; Vatamanu, J.; Ji, X.; Pollard, T. P.; Cui, C.; Hou, S.;

Chen, J.; Yang, C., et al. A 63 m superconcentrated aqueous electrolyte for high-energy Li-ion batteries. *ACS Energy Letters* **2020**, *5*, 968–974.

(18) Graham, T. R.; Dembowski, M.; Wang, H.-W.; Mergelsberg, S. T.; Nienhuis, E. T.; Reynolds, J. G.; Delegard, C. H.; Wei, Y.; Snyder, M.; Leavy, I. I., et al. Hydroxide promotes ion pairing in the NaNO 2–NaOH–H 2 O system. *Physical Chemistry Chemical Physics* **2021**, *23*, 112–122.

(19) Peterson, R. A.; Buck, E. C.; Chun, J.; Daniel, R. C.; Herting, D. L.; Ilton, E. S.; Lumetta, G. J.; Clark, S. B. Review of the scientific understanding of radioactive waste at the US DOE Hanford Site. *Environmental science & technology* **2018**, *52*, 381–396.

(20) Pluharova, E.; Laage, D.; Jungwirth, P. Size and origins of long-range orientational water correlations in dilute aqueous salt solutions. *The Journal of Physical Chemistry Letters* **2017**, *8*, 2031–2035.

(21) Howe, R.; Howells, W.; Enderby, J. Ion distribution and long-range order in concentrated electrolyte solutions. *Journal of Physics C: Solid State Physics* **1974**, *7*, L111.

(22) Marques, M. A.; Cabaço, M.; de Barros Marques, M.; Gaspar, A. Intermediate-range order in aqueous solutions of salts constituted of divalent ions combined with monovalent counter-ions. *Journal of Physics: Condensed Matter* **2002**, *14*, 7427.

(23) Ribeiro, M. C. Intermediate-range order in aqueous solutions of salts: a systematic computer simulation study. *Journal of Physics: Condensed Matter* **2005**, *17*, 453.

(24) Ribeiro, M. C. Intermediate-range order and collective dynamics in an aqueous solution of trivalent cations. *Physical Review B* **2006**, *73*, 014201.

(25) Amann-Winkel, K.; Bellissent-Funel, M.-C.; Bove, L. E.; Loerting, T.; Nilsson, A.; Paciaroni, A.; Schlesinger, D.; Skinner, L. X-ray and Neutron Scattering of Water. *Chemical Reviews* **2016**, *116*, 7570–7589, PMID: 27195477.

(26) Narten, A. H.; Thiessen, W. E.; Blum, L. Atom Pair Distribution Functions of Liquid Water at 25°C from Neutron Diffraction. *Science* **1982**, *217*, 1033–1034.

(27) Leberman, R.; Soper, A. Effect of high salt concentrations on water structure. *Nature* **1995**, *378*, 364–366.

(28) Mancinelli, R.; Botti, A.; Bruni, F.; Ricci, M.; Soper, A. Perturbation of water structure due to monovalent ions in solution. *Physical Chemistry Chemical Physics* **2007**, *9*, 2959–2967.

(29) Zhang, C.; Yue, S.; Panagiotopoulos, A. Z.; Klein, M. L.; Wu, X. Dissolving salt is not equivalent to applying a pressure on water. *Nature communications* **2022**, *13*, 1–6.

(30) Botti, A.; Bruni, F.; Imberti, S.; Ricci, M.; Soper, A. Ions in water: The microscopic structure of concentrated NaOH solutions. *The Journal of chemical physics* **2004**, *120*, 10154–10162.

(31) Skinner, L.; Galib, M.; Fulton, J.; Mundy, C.; Parise, J.; Pham, V.-T.; Schenter, G.; Benmore, C. The structure of liquid water up to 360 MPa from x-ray diffraction measurements using a high Q-range and from molecular simulation. *The Journal of chemical physics* **2016**, *144*, 134504.

(32) Walrafen, G. E. Raman spectral studies of the effects of electrolytes on water. *The Journal of Chemical Physics* **1962**, *36*, 1035–1042.

(33) Soper, A. K.; Weckström, K. Ion solvation and water structure in potassium halide aqueous solutions. *Biophysical chemistry* **2006**, *124*, 180–191.

(34) Gallo, P.; Corradini, D.; Rovere, M. Do ions affect the structure of water? The case of potassium halides. *Journal of Molecular Liquids* **2014**, *189*, 52–56.

(35) Hellström, M.; Behler, J. Structure of aqueous NaOH solutions: insights from neural-network-based molecular dynamics simulations. *Phys. Chem. Chem. Phys.* **2017**, *19*, 82–96.

(36) Timmons, A.; Symes, M. Converting between the oxides of nitrogen using metal–ligand coordination complexes. *Chem. Soc. Rev.* **2015**, *44*.

(37) Toby, B. H.; Von Dreele, R. B. GSAS-II: the genesis of a modern open-source all purpose crystallography software package. *Journal of Applied Crystallography* **2013**, *46*, 544–549.

(38) Qiu, X.; Thompson, J. W.; Billinge, S. J. L. *PDFgetX2*: a GUI-driven program to obtain the pair distribution function from X-ray powder diffraction data. *Journal of Applied Crystallography* **2004**, *37*, 678.

(39) Proffen, T.; Neder, R. B. *DISCUS*: a program for diffuse scattering and defect-structure simulation. *Journal of Applied Crystallography* **1997**, *30*, 171–175.

(40) Megyes, T.; Bálint, S.; Peter, E.; Grosz, T.; Bakó, I.; Krienke, H.; Bellissent-Funel, M.-C. Solution structure of NaNO3 in water: Diffraction and molecular dynamics simulation study. *The Journal of Physical Chemistry B* **2009**, *113*, 4054–4064.

(41) Gagné, O. C.; Hawthorne, F. C. Bond-length distributions for ions bonded to oxygen: alkali and alkaline-earth metals. *Acta Crystallographica Section B: Structural Science, Crystal Engineering and Materials* **2016**, *72*, 602–625.

(42) Lalitha, M.; Senthilkumar, L. DFT study on X-·(H2O) n= 1-10 (X= OH, NO2, NO3, CO3) anionic water cluster. *Journal of Molecular Graphics and Modelling* **2014**, *54*, 148–163.

(43) Yadav, S.; Chandra, A. Solvation shell of the nitrite ion in water: an ab initio molecular dynamics study. *The Journal of Physical Chemistry B* **2020**, *124*, 7194–7204.

(44) Reynolds, J. G.; Mauss, B. M.; Daniel, R. C. The relative viscosity of NaNO3 and NaNO2 aqueous solutions. *Journal of Molecular Liquids* **2018**, *264*, 110–114.

(45) Saxena, P.; Thirupathi, N. Reactions of Cd (OAc) 2· 2H2O with variously substituted pyridines. Efforts to unravel the factors that determine structure/nuclearity of the products. *Polyhedron* **2015**, *98*, 238–250.